AFRL-RX-WP-JA-2015-0185

MICROSTRUCTURE OF ZNO THIN FILMS DEPOSITED BY HIGH POWER IMPULSE MAGNETRON SPUTTERING (POSTPRINT)

A. N. Reed and A. A. Voevodin
AFRL/RXAN

C. Muratore
Department of Chemical and Materials Engineering, University of Dayton

P. J. Shamberger
Texas A&M University

J. J. Hu and J. E. Bultman
University of Dayton Research Institute, University of Dayton

MARCH 2015
Interim Report

Approved for public release; distribution unlimited.

See additional restrictions described on inside pages

STINFO COPY

AIR FORCE RESEARCH LABORATORY
MATERIALS AND MANUFACTURING DIRECTORATE
WRIGHT-PATTERSON AIR FORCE BASE, OH 45433-7750
AIR FORCE MATERIEL COMMAND
UNITED STATES AIR FORCE

NOTICE AND SIGNATURE PAGE

Using Government drawings, specifications, or other data included in this document for any purpose other than Government procurement does not in any way obligate the U.S. Government. The fact that the Government formulated or supplied the drawings, specifications, or other data does not license the holder or any other person or corporation; or convey any rights or permission to manufacture, use, or sell any patented invention that may relate to them.

This report was cleared for public release by the USAF 88th Air Base Wing (88 ABW) Public Affairs Office (PAO) and is available to the general public, including foreign nationals.

Copies may be obtained from the Defense Technical Information Center (DTIC) (http://www.dtic.mil).

AFRL-RX-WP-JA-2015-0185 HAS BEEN REVIEWED AND IS APPROVED FOR PUBLICATION IN ACCORDANCE WITH ASSIGNED DISTRIBUTION STATEMENT.

//Signature//

AMBER N. REED
Nanoelectronic Materials Branch
Functional Materials Division

//Signature//

DIANA M. CARLIN, Chief
Nanoelectronic Materials Branch
Functional Materials Division

//Signature//

KAREN R. OLSON, Actg Chief
Functional Materials Division
Materials and Manufacturing Directorate

This report is published in the interest of scientific and technical information exchange, and its publication does not constitute the Government's approval or disapproval of its ideas or findings.

REPORT DOCUMENTATION PAGE

Form Approved OMB No. 074-0188

Public reporting burden for this collection of information is estimated to average 1 hour per response, including the time for reviewing instructions, searching existing data sources, gathering and maintaining the data needed, and completing and reviewing this collection of information. Send comments regarding this burden estimate or any other aspect of this collection of information, including suggestions for reducing this burden to Defense, Washington Headquarters Services, Directorate for Information Operations and Reports, 1215 Jefferson Davis Highway, Suite 1204, Arlington, VA 22202-4302. Respondents should be aware that notwithstanding any other provision of law, no person shall be subject to any penalty for failing to comply with a collection of information if it dows not display a currently valid OMB control number. PLEASE DO NOT RETURN YOUR FORM TO THE ABOVE ADDRESS.

1. REPORT DATE (DD-MM-YYYY)
March 2015

2. REPORT TYPE
Interim

3. DATES COVERED *(From – To)*
29 January 2013 – 16 February 2015

4. TITLE AND SUBTITLE
MICROSTRUCTURE OF ZNO THIN FILMS DEPOSITED BY HIGH POWER IMPULSE MAGNETRON SPUTTERING (POSTPRINT)

5a. CONTRACT NUMBER
FA8650-11-D-5401-0011

5b. GRANT NUMBER

5c. PROGRAM ELEMENT NUMBER
62102F

6. AUTHOR(S)
(see back)

5d. PROJECT NUMBER
4348

5e. TASK NUMBER

5f. WORK UNIT NUMBER
X0K9

7. PERFORMING ORGANIZATION NAME(S) AND ADDRESS(ES)
(see back)

8. PERFORMING ORGANIZATION REPORT NUMBER

9. SPONSORING / MONITORING AGENCY NAME(S) AND ADDRESS(ES)
Air Force Research Laboratory
Materials and Manufacturing Directorate
Wright Patterson Air Force Base, OH 45433-7750
Air Force Materiel Command
United States Air Force

10. SPONSOR/MONITOR'S ACRONYM(S)
AFRL/RXAN

11. SPONSOR/MONITOR'S REPORT NUMBER(S)
AFRL-RX-WP-JA-2015-0185

12. DISTRIBUTION / AVAILABILITY STATEMENT
Approved for public release; distribution unlimited. This report contains color.

13. SUPPLEMENTARY NOTES
PA Case Number: 88ABW-2014-3153; Clearance Date: 30 June 2014. Journal article published in Thin Solid Films 579 (2015) 30-37. The U.S. Government is joint author of the work and has the right to use, modify, reproduce, release, perform, display or disclose the work. The final publication is available at http://dx.doi.org/10.1016/j.tsf.2015.02.048.

14. ABSTRACT
High power impulse magnetron sputtering was used to deposit thin (~100 nm) zinc oxide (ZnO) films from a ceramic ZnO target onto substrates heated to 150 °C. The resulting films had strong crystallinity, highly aligned (002) texture and low surface roughness (root mean square roughness less than 10 nm), as determined by X-ray diffraction, transmission electronmicroscopy, scanning electron microscopy and atomic force spectroscopy measurements. Deposition pressure and target–substrate distance had the greatest effect on film microstructure. The degree of alignment in the films was strongly dependent on the gas pressure. Deposition at pressures less than 0.93 Pa resulted in a bimodal distribution of grain sizes. An initial growth layer with preferred orientations (101) and (002) parallel to the interface was observed at the film–substrate interface under all conditions examined here; the extent of that competitive region was dependent on growth conditions. Time-resolved current measurements of the target and ion energy distributions, determined using energy resolved mass spectrometry, were correlated to film microstructure in order to investigate the effect of plasma conditions on film nucleation and growth.

15. SUBJECT TERMS
HiPIMS, ZnO, low-temperature deposition, sputtering, microstructure

16. SECURITY CLASSIFICATION OF:			17. LIMITATION OF ABSTRACT	18. NUMBER OF PAGES	19a. NAME OF RESPONSIBLE PERSON *(Monitor)*
					Amber N. Reed
a. REPORT	**b. ABSTRACT**	**c. THIS PAGE**	SAR	12	**19b. TELEPHONE NUBER** *(include area code)*
Unclassified	Unclassified	Unclassified			(937) 255-5501

Standard Form 298 (Rev. 2-89)
Prescribed by ANSI Std. Z39-18

REPORT DOCUMENTATION PAGE Cont'd

6. AUTHOR(S)

A. N. Reed and A. A. Voevodin - Materials and Manufacturing Directorate, Air Force Research Laboratory
C. Muratore - Department of Chemical and Materials Engineering, University of Dayton
P. J. Shamberger - Department of Materials Science and Engineering, Texas A&M University
J. J. Hu and J. E. Bultman - University of Dayton Research Institute, University of Dayton

7. PERFORMING ORGANIZATION NAME(S) AND ADDRESS(ES)

AFRL/RXAN
Air Force Research Laboratory
Materials and Manufacturing Directorate
Wright-Patterson Air Force Base, OH 45433-7750

Department of Chemical and Materials Engineering
University of Dayton
Dayton, OH 45469

Department of Materials Science and Engineering
Texas A&M University
College Station, TX 77843

University of Dayton Research Institute
University of Dayton
Dayton, OH 45469

Thin Solid Films 579 (2015) 30–37

Contents lists available at ScienceDirect

Thin Solid Films

journal homepage: www.elsevier.com/locate/tsf

Microstructure of ZnO thin films deposited by high power impulse magnetron sputtering

A.N. Reed [a,b,*], P.J. Shamberger [c], J.J. Hu [a,d], C. Muratore [b], J.E. Bultman [a,d], A.A. Voevodin [a,**]

[a] Materials and Manufacturing Directorate, Air Force Research Laboratory, 3005 Hobson Way, Wright Patterson Air Force Base, OH 45433, USA
[b] Department of Chemical and Materials Engineering, University of Dayton, Dayton, OH 45469, USA
[c] Department of Materials Science and Engineering, Texas A&M University, College Station, TX 77843, USA
[d] University of Dayton Research Institute, University of Dayton, Dayton, OH 45469, USA

ARTICLE INFO

Article history:
Received 30 June 2014
Received in revised form 12 February 2015
Accepted 16 February 2015
Available online 21 February 2015

Keywords:
HiPIMS
ZnO
Low-temperature deposition
Sputtering
Microstructure

ABSTRACT

High power impulse magnetron sputtering was used to deposit thin (~100 nm) zinc oxide (ZnO) films from a ceramic ZnO target onto substrates heated to 150 °C. The resulting films had strong crystallinity, highly aligned (002) texture and low surface roughness (root mean square roughness less than 10 nm), as determined by X-ray diffraction, transmission electron microscopy, scanning electron microscopy and atomic force spectroscopy measurements. Deposition pressure and target–substrate distance had the greatest effect on film microstructure. The degree of alignment in the films was strongly dependent on the gas pressure. Deposition at pressures less than 0.93 Pa resulted in a bimodal distribution of grain sizes. An initial growth layer with preferred orientations (101) and (002) parallel to the interface was observed at the film–substrate interface under all conditions examined here; the extent of that competitive region was dependent on growth conditions. Time-resolved current measurements of the target and ion energy distributions, determined using energy resolved mass spectrometry, were correlated to film microstructure in order to investigate the effect of plasma conditions on film nucleation and growth.

Published by Elsevier B.V.

1. Introduction

Zinc oxide (ZnO) is an important semiconductor material with an intriguing combination of high mobility and wide band gap, allowing for high frequency operation and high transistor channel on–off ratios. These properties make ZnO attractive as a channel material for a variety of optoelectronic and transparent thin film field effect transistor (TFT) devices used in active displays, solar cells, chem- and bio-sensors, radio frequency (RF) signal processing, power electronics and other applications [1–3]. A variety of deposition techniques have been used to grow ZnO films, including chemical vapor deposition [4,5], atomic layer deposition [6], solution based hydrothermal deposition [7], filtered vacuum cathodic arc deposition [8–10], pulsed laser deposition (PLD) [11–17], RF sputtering [18–22], direct current (DC) and pulsed DC magnetron sputtering [23,24] and high power impulse magnetron sputtering (HiPIMS) [25,26].

The electrical properties that determine device performance for TFTs can be strongly dependent on the microstructural properties of the film. For example, the highest field effect mobilities, up to 110 $cm^2 V^{-1} s^{-1}$, and on–off ratios, up to 10^{12}, reported for ZnO thin film transistors have been for devices where the channel was composed of nanocrystalline wurtzite ZnO, deposited using PLD [27]. To achieve a high carrier mobility, PLD processing has shown a need for ZnO films to have a low surface roughness, dense morphology and a strong (002) orientation [27–29]. In these studies the growth temperatures of about 350 °C and subsequent thin film annealing were used to obtain the desired film surface morphology and crystallinity needed for the charge transport properties. To extend ZnO applications to flexible polymer substrates, a reduction of the growth temperature is needed. In addition, there are intrinsic challenges to the scalability of PLD thin film growth to coat large area and complex-shaped substrates, which motivates investigation of other techniques for the low temperature and scalable deposition of ZnO films while using the material morphology and structure optimization identified with the PLD growth studies. From this perspective, magnetron sputtering techniques with energetic plasma fluxes hold a great deal of potential for scalability of ZnO synthesis at low temperatures. However, initial investigations with conventional magnetron sputtering reported in literature yield ZnO films with low mobilities (μ_{FE} $\leq$1.8 $cm^2 V^{-1} s^{-1}$) [30], due to poor crystallinity, open columnar structure with a high degree of porosity, and random crystallographic

* Correspondence to: A.N. Reed, Materials and Manufacturing Directorate, Air Force Research Laboratory, 3005 Hobson Way, Wright Patterson Air Force Base, OH 45433, USA. Tel.: +1 937 255 4651.
** Corresponding author. Tel.: +1 937 255 4651
E-mail addresses: amber.reed.5@us.af.mil (A.N. Reed), andrey.voevodin@us.af.mil (A.A. Voevodin).

http://dx.doi.org/10.1016/j.tsf.2015.02.048
0040-6090/Published by Elsevier B.V.

Distribution Statement A. Approved for public release; distribution unlimited.

orientation. The higher ion fluxes and ion energies [31,32] associated with HiPIMS make it an alternative scalable technique to grow ZnO with controlled microstructures and crystallographic orientation needed to alter film microstructures to improve electrical transport properties.

Reactive HiPIMS of Zn targets in an argon-oxygen background has previously been demonstrated to deposit ZnO films on glass [25] and sapphire [26] substrates. The ZnO films grown on both substrate materials were nanocrystalline with small ~30 nm size grains with the (002) plane oriented parallel to the substrate. These films had a surface roughness below 1.0 nm and lower porosity than ZnO films grown with dc bipolar magnetron sputtering [25]. The deposition rates of HiPIMS and DC sputtering were similar when HiPIMS was operated with short 10 μs [25] and 50 μs [26] pulses. The feasibility of reactive HiPIMS for the deposition of ZnO thin films for electronics was tested by Partridge et al. [26] by measuring the films' Hall mobility and the I–V characteristics of the ZnO film in a diode. The as-deposited films had Hall mobilities of 7–8 $cm^2 V^{-1} s^{-1}$, which is significantly lower than the Hall mobilities of >50 $cm^2 V^{-1} s^{-1}$ reported for ZnO films grown with PLD [27]. Thus, the use of HiPIMS deposited ZnO films as a TFT channel material needs further investigation. In particular, detailed studies of the effect of HiPIMS deposition parameters on film microstructure and an understanding of the film growth mechanisms to control density and desired (002) texture could yield an improvement in the films' mobility.

In this work, ZnO films grown using HiPIMS from an oxide target were investigated to determine the role of growth conditions on film development. The nucleation and growth mechanisms are identified and correlated to the deposition conditions. Special focus was paid to the role of deposition pressure and ion fluxes on ZnO film growth rate, surface roughness, grain size and crystal orientation.

1.1. Experimental details

In this study all experiments were performed in the ultra-high vacuum system, shown in Fig. 1, at base pressures less than $1.33 * 10^{-5}$ Pa. The plasma was driven with a Huettinger HMP-1200 HiPIMS power supply controlling the voltage applied to a 5.08 cm diameter ZnO target.

Time-resolved target voltages and currents were measured using a Tektronix P5200 high voltage differential probe and a Tektronix TMA502A current probe, respectively, and recorded with a Tektronix TDS 5400 oscilloscope. Ion energy distributions (IEDs) for argon, oxygen, zinc and zinc oxide were measured using an energy-resolved Hiden EQP 1000 electrostatic quadrupole (EQP) mass spectrometer. To facilitate these measurements, the substrate holder was removed from the chamber and the grounded orifice of the EQP was positioned 10 cm from the face of the target. Fig. 1b shows the arrangement of the chamber during the IED measurements. IEDs were measured for mass-charge ratios of 16 amu/C(O^+), 32 amu/C(O_2^+), 40 amu/C(Ar^+), 64 amu/C(Zn^+) and 80 amu/C(ZnO^+). Scans were taken with a dwell time of 300 ms so each data point was composed of 30 pulses.

ZnO films were deposited onto conductive silicon wafers (ρ = 1–10 Ω cm) with a 100 nm thick SiO_2 layer. Before deposition the substrates were sonicated in acetone, rinsed, sonicated with methanol, rinsed with ultra-pure H_2O and dried with nitrogen. The target to substrate distance was either 5 cm or 10 cm. During the depositions, the grounded substrates were heated to 150 °C and rotated to promote

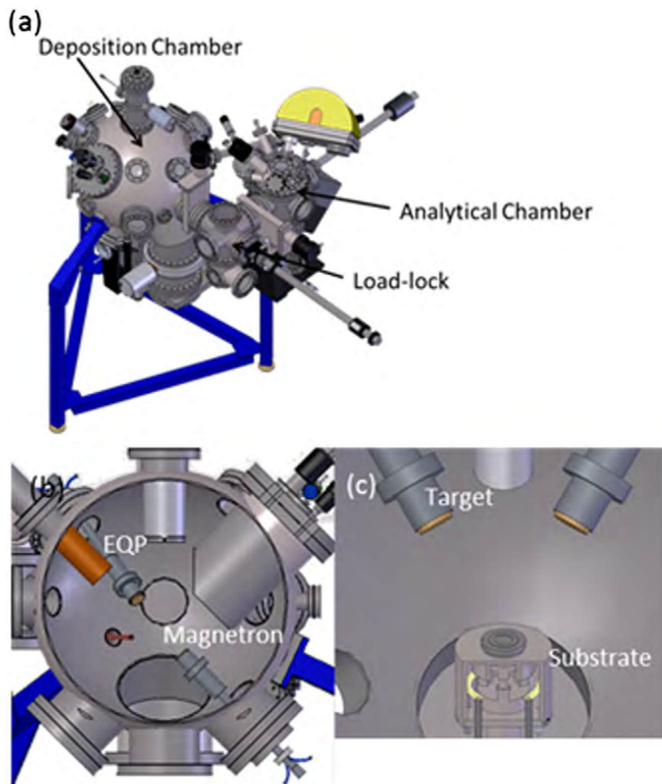

Fig. 1. Schematic of (a) exterior and (b) interior of deposition chamber configured for energy-resolved mass spectrometry and (c) the arrangement of the chamber for depositions.

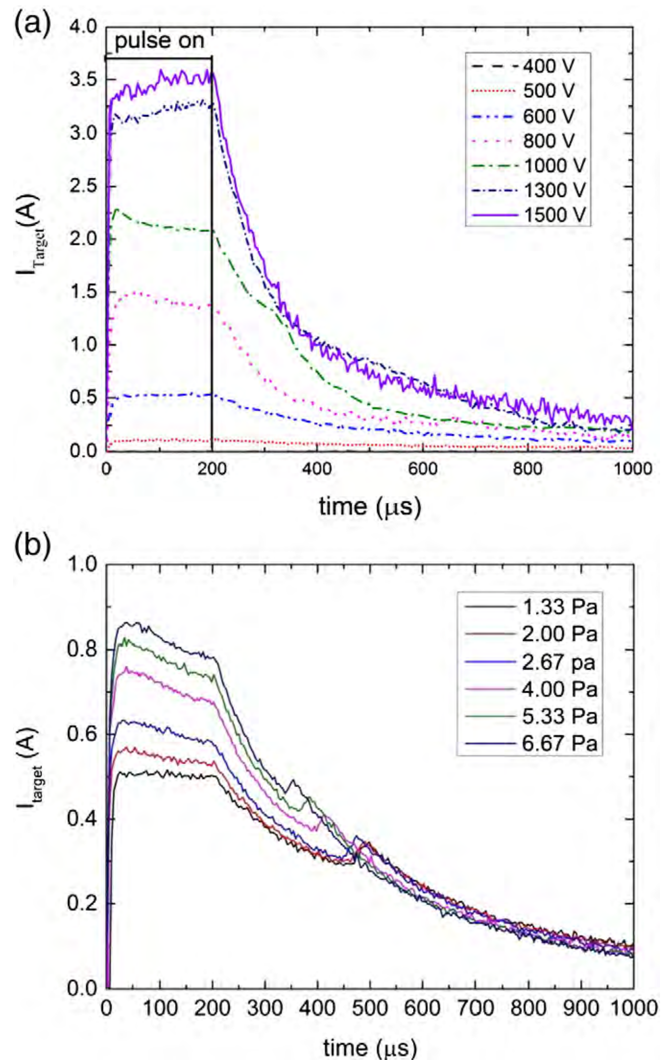

Fig. 2. Time-resolved target current for ZnO target during HiPIMS with (a) different applied target voltages at a pressure of 2.67 Pa and (b) 650 V pulses at different pressures. The pulses in both (a) and (b) were 200 μs and a ratio of O_2 and Ar flow rates of 0.04 was used.

Distribution Statement A. Approved for public release; distribution unlimited.

film uniformity. Films were deposited in 0.40–6.67 Pa oxygen–argon gas mixture; the O_2/Ar was held at 0.04 with an argon flow rate of 25 sccm and an oxygen flow rate of 1 sccm. The HiPIMS power supply applied 1500 V to the target with either 50 μs or 200 μs pulses at a frequency of 100 Hz. The total deposition time for each sample was adjusted to obtain films approximately 100 nm thick (±10%) at all selected deposition conditions.

A small section of the substrate was masked during deposition, allowing for film thickness measurement by a KLA Tencor P-15 stylus profilometer with a 2 μm diameter probe tip. Parallel beam wide angle x-ray diffraction (XRD) and rocking curve measurements of the films were performed using a Rigaku Smartlab XRD system with a Cu anode. Beam divergence was minimized using a 1 mm divergence slit and a 0.5° parallel slit analyzer. Rocking curve measurements were collected with the detector angle corresponding to the maximum intensity of the ZnO (002) peak (2θ = 34.0° to 34.6°). Film cross-sections were imaged using a Sirion scanning electron microscope (SEM) with a through-lens-detector, an acceleration voltage of 5.0 kV and working distances of 4.5–7.0 mm. An FEI Nova focused ion beam (FIB) microscope equipped with an Omniprobe manipulator was employed to prepare transmission electron microscope (TEM) specimens to analyze the cross-sectional microstructure of the films. The FIB microscope was operated using 5 kV electron beams and 30 kV Ga^+ ion beams. High-resolution microstructures were observed using a FEI TitanTM 80–300 S/TEM, which was equipped with a Cs-corrector and was operated at 300 kV. Energy-dispersive X-ray spectroscopy and electron energy loss spectroscopy were employed for chemistry measurements in the TEM. Surface features and roughness of the films were examined with atomic force microscopy (AFM) in tapping mode with a scan rate of 0.5 Hz using an Asylum MFP-3D AFM with an Asylum AC160TS Si

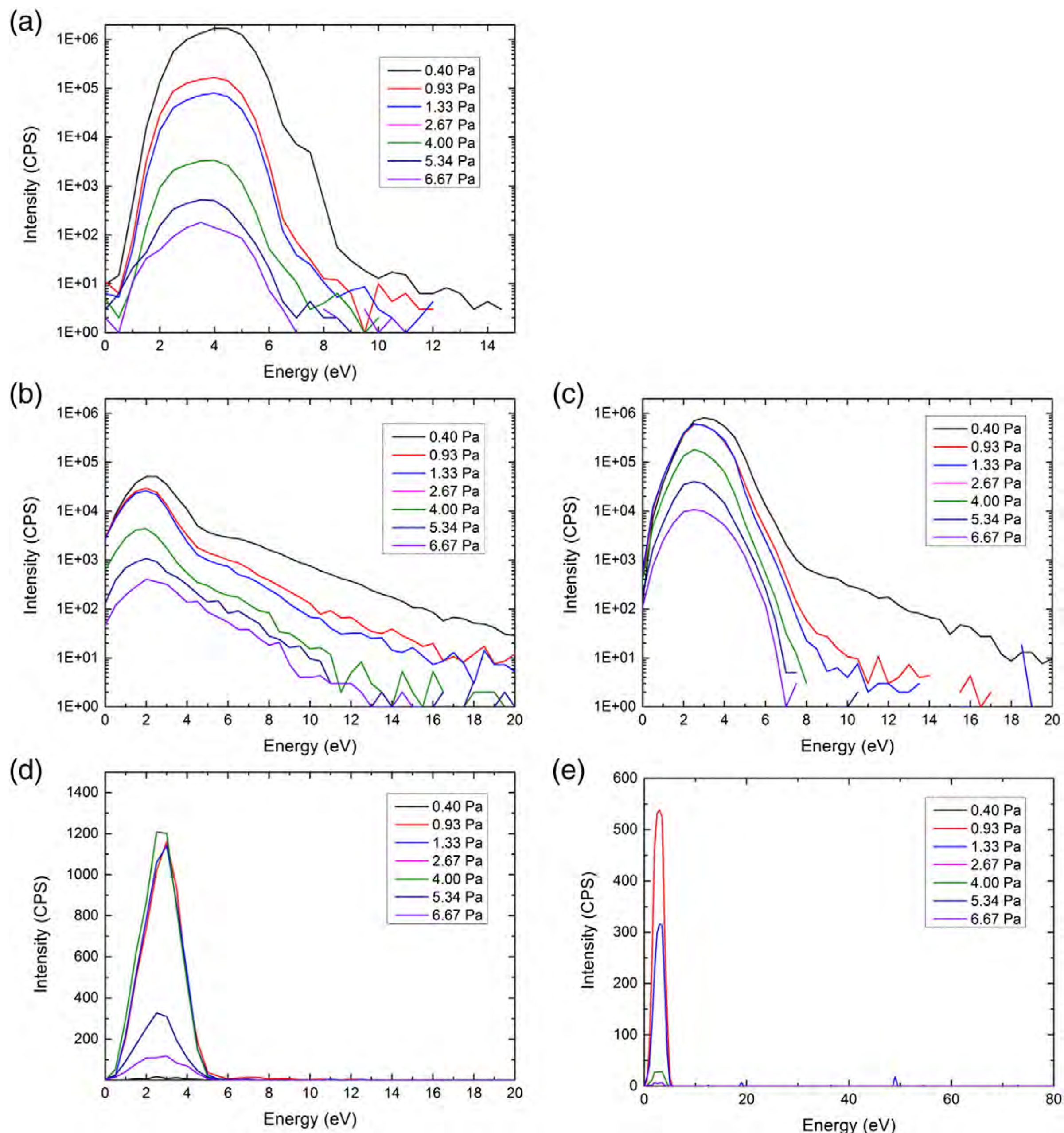

Fig. 3. Measured ion energy distributions for (a) Ar^+, (b) O^+, O_2^{++}, (c) O_2^+, (d) Zn^+ and (e) ZnO^+ at different total pressures with a fixed O_2/Ar of 0.04. The scans had a dwell time of 300 ms while HiPIMS supply applied 50 μs pulses at a frequency of 100 Hz to the target.

Distribution Statement A. Approved for public release; distribution unlimited.

cantilever. The cantilever had a resonant frequency of 300 kHz and a nominal tip radius of 9 ± 2 nm.

2. Results

The representative target currents for different applied voltages and total pressures can be seen in Fig. 2. The current rose immediately after pulse initiation; the peak current value and behavior during the pulse were dependent on pressure and applied voltage. Three distinct current–time behaviors were observed during the pulse. Low applied voltages (≤600 V) and low pressure (≤1.33 Pa) resulted in a current that reached its peak value and plateaued shortly after pulse initiation. The lowest applied voltage (V = 400 V) produced weak plasma glow at the target surface and a current of <1 mA during the pulse, reflecting a very small ion flux to the target. Films grown in this regime had poor crystallinity and a broad low intensity ZnO (002) diffraction peak, suggesting that the depositing flux at the substrate had insufficient energy to promote crystallization. At intermediate voltage (650–1000 V) and pressures >1.33 Pa the current reached its peak value at the beginning of the pulse then decreased to a steady state value as rarefaction [33] of the process gas adjacent to the target occurred and the flux of available gas ions near the target surface reduced. At higher voltages of >1000 V, sufficient ionization of the sputtered atoms occurred to counteract rarefaction and the target current increased for the entire duration of the pulse.

A subsequent rise in target current was observed at 100–300 μs after termination of the applied pulse, with the occurrence of this second current peak being delayed with decreasing pressure. We believe that this secondary pulse is the result of ionized target material incident on the target [34]. The pressure dependence on time at which this pulse appears is likely determined by the mean free path of the material after liberation from the target.

The IEDs for Ar^+, O^+, O_2^+, O^{2+}, Zn^+ and ZnO^+ are shown in Fig. 3. The intensities, which are proportional to the total flux, for the gas ion species were 2–3 orders of magnitude higher than those of the target ions. At a pressure of 0.40 Pa, the IED for argon had a most probable ion energy of 4 eV and a maximum ion energy of about 15 eV. Both the flux and its rate of decay decreased with increasing pressure. The next most abundant species comprising the flux was O_2^+ (Fig. 3c) with a peak at ~3.5 eV and a higher energy tail. As with the oxygen, the flux decreased with increased pressure. The O^+/O_2^{++} IED (Fig. 3b) showed similar behavior though it had an order of magnitude lower intensity. The IEDs for the oxygen ions extended to approximately 20 eV compared to 15 eV for argon ions. The IED for Zn^+ had a single peak centered at 3 eV and was weakly dependent on pressure in comparison to the gas ions; little change in intensity was observed until the pressure exceeded 4.00 Pa then the counts sharply dropped to at 5.33 Pa and higher pressures. The Zn^+ IED in Fig. 3d shows less relative metal ionization in comparison to other ionized species than typically observed in HiPIMS for metallic targets [35–37]. This lack of Zn ionization is likely due to the relatively lower peak currents during sputtering, I_{target} > 3.5 A for the compound target compared to values >50 A reported in literature for metallic targets [38–40]. The flux of ZnO^+ ions was lower than the detectable limits of the EQP. Negative oxygen ions reported during sputtering of ZnO [41–43] and HiPIMS of other oxides [44] were not found in our study or were below the detection limit of the instrumentation arrangements.

Fig. 4 illustrates results from wide angle XRD as a function of pressure for films grown with 200 μs (Fig. 4a) and 50 μs (Fig. 4b) pulses. Two diffraction peaks were present, ZnO (002) at 2θ = 34.3° and ZnO (101) at 2θ = 36.0°. The (101) diffraction peak was two orders of magnitude less intense than the (002) peak for all the films. As pressure decreases, the (002) wide angle diffraction peak broadens. This result is most visible at pressures below 1.33 Pa. The broadening of the (002) peak at 0.67 Pa was less pronounced for the 50 μs film compared to the 200 μs. The vertical axis in Fig. 4c represents integrated intensity

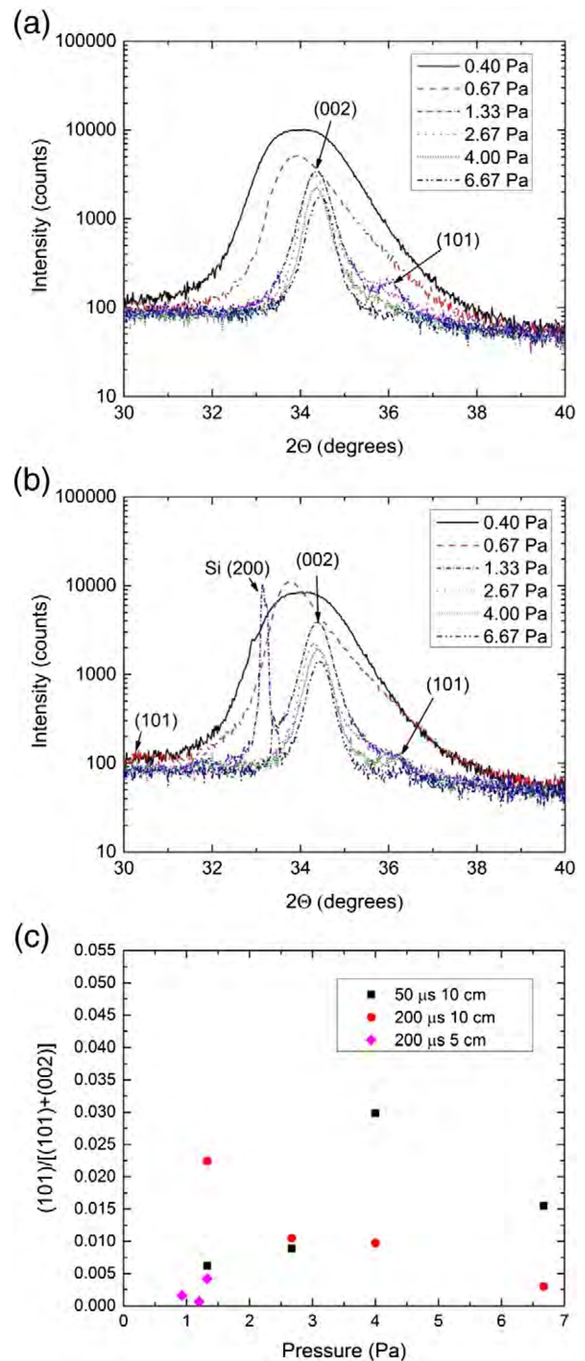

Fig. 4. Wide angle XRD for ZnO films grown with (a) 200 μs and (b) 50 μs pulses at different Ar/O_2 pressures. The *y*-axis is plotted in log scale for clarity. Wide angle scans were performed from 2θ = 25–80°, but the *x*-axis is scaled to best show the region containing the (100), (002) and (101) peaks. (c) Ratio of the area of the (101) peak to the total area of the (101) and (002) peaks from the wide angle XRD scan plotted against pressure.

of the (101) peak divided by the sum of these for the (101) and (002) peaks. Considering both the 50 μs and 200 μs data, no significant relationship between deposition pressure and (101) texture appearance was observed. Reducing the substrate to target distance from 10 cm to 5 cm, decreased the fraction of (101) oriented grains, with an average diffraction intensity ratio $I_{(101)}/[I_{(101)}+I_{(002)}]$ of 0.004 compared to 0.047 for the films grown at 1.33 Pa.

Fig. 5 shows the rocking curve measurements for the films characterized in Fig. 4. For both the 200 μs and 50 μs films the rocking curves became broader with increased pressure. The vertical axis of Fig. 5c shows the full width half maximum (FWHM) of the (002) rocking

Distribution Statement A. Approved for public release; distribution unlimited.

curves. The rocking curve FWHM for all the films increased with pressure. The narrowest FWHMs occurred when the pressure was below 1.33 Pa, where FWHM appears to be most sensitive to pressure changes.

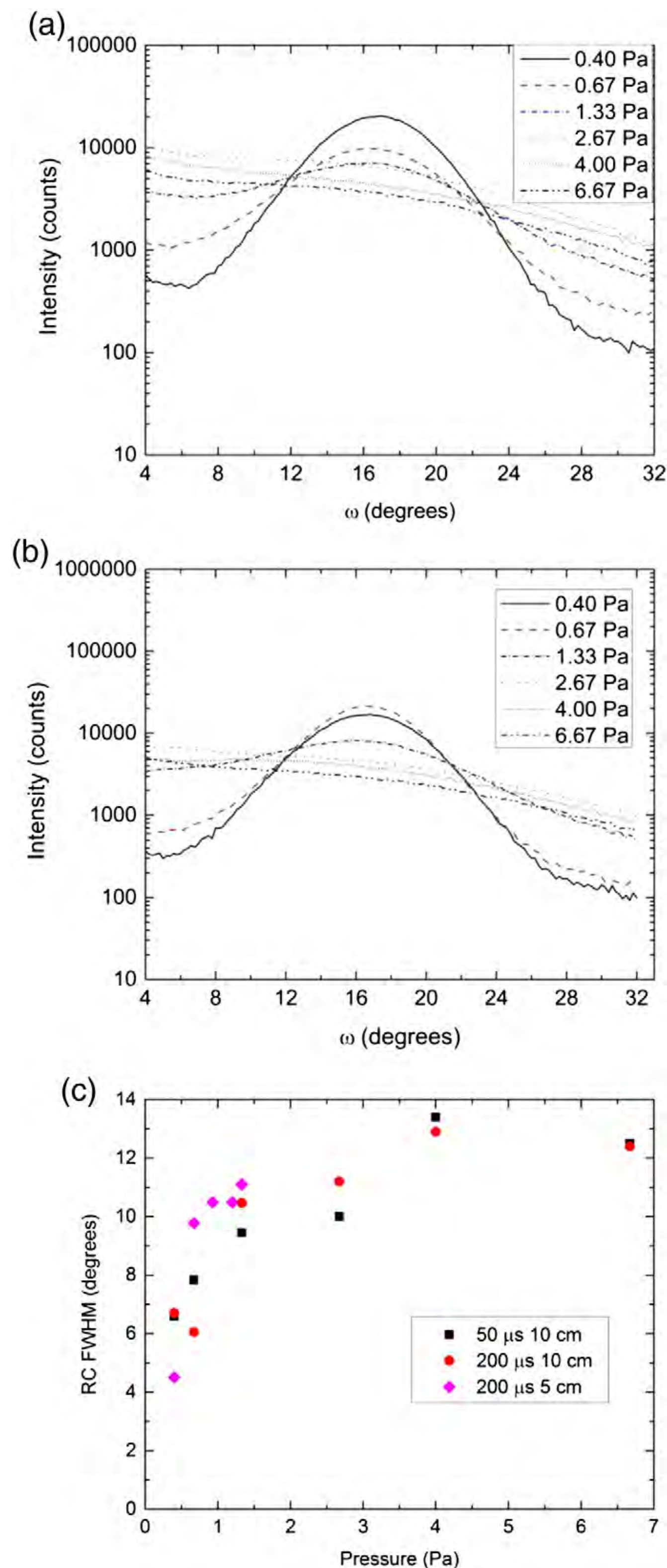

Fig. 5. Rocking curve XRD of the (002) peak for ZnO films grown with (a) 200 μs and (b) 50 μs pulses at different Ar/O_2 pressures. The *y*-axis is plotted in log scale for clarity. (c) Full width half maximum of the (002) rocking curve peak of HiPIMS-grown ZnO films plotted as a function of deposition pressure.

The FWHM of the 200 μs film at 0.40 Pa is only 6.58°, while the FWHM at 1.33 Pa is 9.45°. For the 50 μs pulse films the rocking curve (Fig. 5b) narrowed from an FWHM of 10.47° at 1.33 Pa to an FWHM of 6.71° at 0.40 Pa. No significant change in the FWHM was observed by shortening the substrate–target distance.

TEM and SEM micrographs of the cross-section of a representative film grown at 1.33 Pa are shown in Fig. 6. Fig. 6a shows a smooth interface between the ZnO film and the amorphous SiO_2 layer on the substrate. No amorphous ZnO layer is observed in the TEM micrograph. The initial ZnO growth at the substrate interface appears to be small V-shaped grains that become narrow columns after the first few tens of nanometers, as evidenced in the SEM micrograph in Fig. 6b.

The TEM cross-section of the film grown at 0.40 Pa is shown in Fig. 7. The yellow lines drawn in Fig. 7 highlight the lattice structures in the TEM micrograph. The micrograph shows that the (002) crystal plane is parallel to the substrate in all grains. The lattice parallel to the substrate has a spacing of 2.607–2.610 Å, slightly larger than the standard value of 2.603 Å. The diagonal lattice, corresponding to diffraction from the (101) plane, has a spacing of 2.633 Å. The (100) plane showed diffraction line perpendicular to the substrate and has a spacing of 2.831 Å, larger than the standard value of 2.814 Å. The dotted white

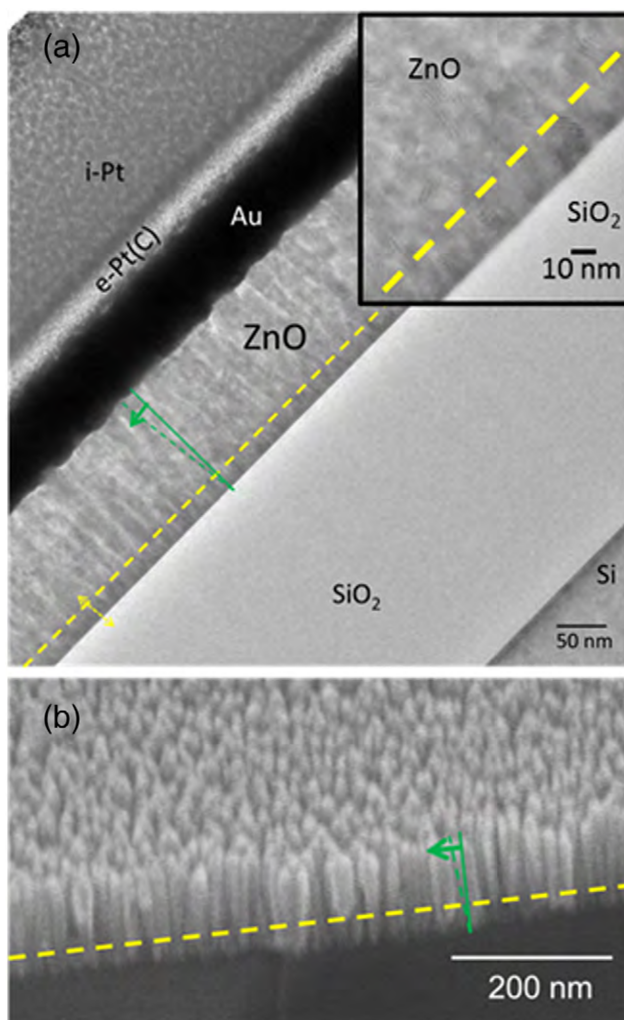

Fig. 6. Cross-sectional (a) TEM with an insert of a close up of the ZnO–SiO_2 interface and (b) SEM of a film grown at 1.33 Pa with a 200 μs pulse length. The yellow-dash line shows the extent of the competitive growth layer and the green line and arrow represent the degree (ω) of the c-axis orientation.

Distribution Statement A. Approved for public release; distribution unlimited.

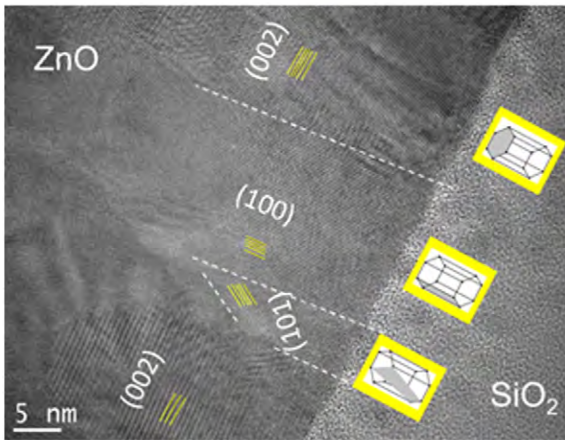

Fig. 7. Cross-sectional TEM of a ZnO film grown with a deposition pressure of 0.40 Pa.

lines in Fig. 7 highlight grain boundaries in the film. The grain with the (101) lattice image is 6 nm across while the (100) grain is 17 nm.

The AFM images of the ZnO film surfaces are presented in Fig. 8 and show that the films are all fairly smooth with RMS roughnesses < 10 nm. The films grown at pressures 1.33 Pa and higher have similar surface topography and surface roughnesses of 4.6–6.1 nm. The difference in surface roughness between the films is comparable to the uncertainty caused by AFM tip dulling during scans. The surface of the film grown at 0.40 Pa has larger grains (~25 nm diameter) intermixed with the smaller grains and a lower surface roughness. AFM topography maps showed that the larger grains were 10–15 nm taller than the smaller grains. Even with the larger grains intermixed among the small grained background, the RMS roughness of the 0.40 Pa film was lower than the other films (RMS roughness = 1.4 nm). ZnO films grown with 50 μs pulses exhibited similar AFM topography (not shown here) with bimodal grain sizes at low pressures (0.40 Pa and 0.67 Pa growth conditions).

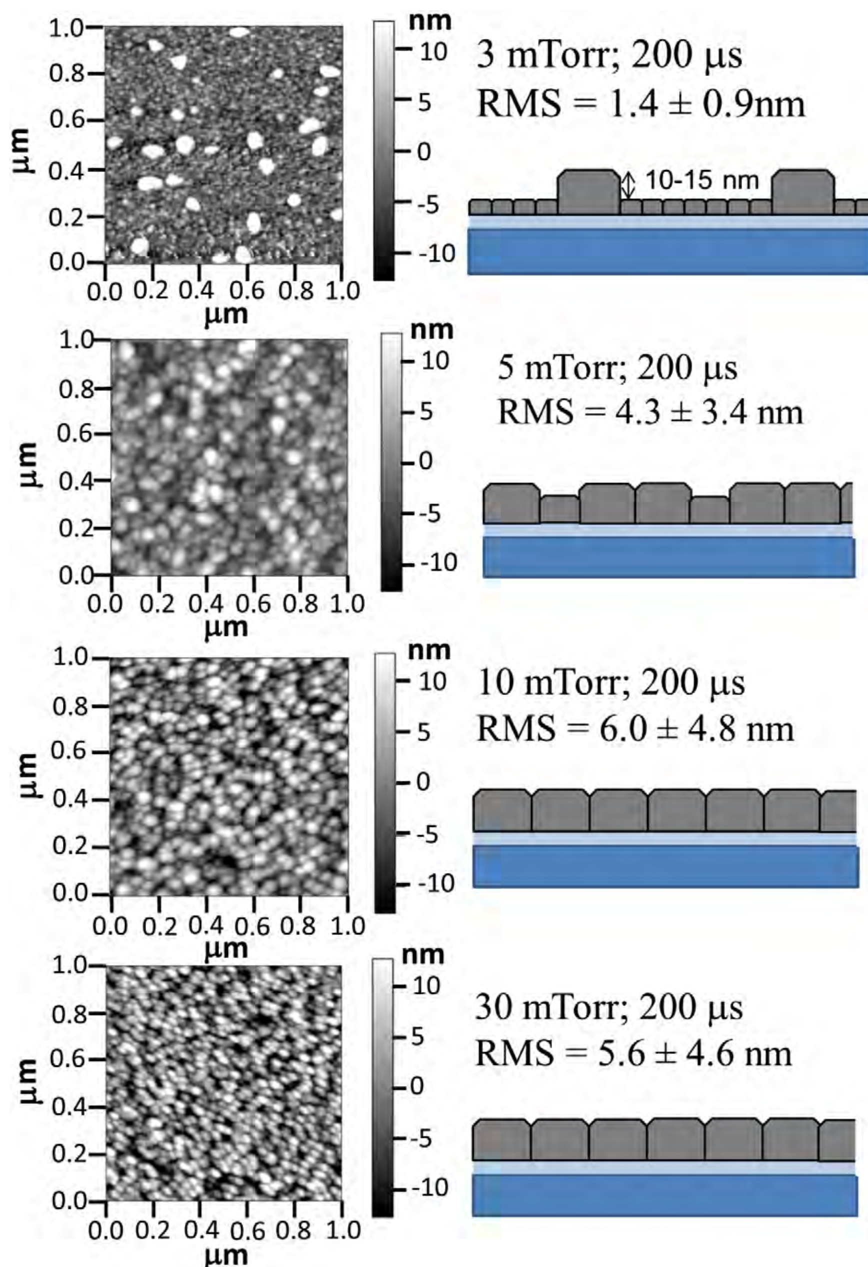

Fig. 8. Surface AFM images and schematic representations of grains in ZnO films grown by HiPIMS with different pressures.

Distribution Statement A. Approved for public release; distribution unlimited.

3. Discussion

The XRD results in Figs. 3 and 4 suggest the columns observed in the SEM in Fig. 5 are composed of grains oriented with (002) parallel to the substrate interface. The film microstructure at the substrate interface, investigated with cross-sectional TEM (Fig. 6a), shows a layer of competitive growth which likely contributes to the low-intensity (101) diffraction in the wide angle XRD at $2\Theta = 36°$. This result is consistent with previous work on ZnO films where polycrystalline competitive growth regions near the substrate–film interface were also found [45,46]. This initial layer is composed primarily of (101) and (002) orientations while there is little to no (100) observed in the XRD patterns which would be expected if the layer had a random orientation. Because the competitive texture layer is located at the film–substrate interface, the location of the depletion zone in a back-gated FET device, it could potentially play an exaggerated role in controlling transistor transport properties. From analysis of the XRD data in Fig. 3c, we infer no correlation between deposition pressure and the extent of the competitive texture layer growth. However, decreasing the substrate to target distance appears to reduce the presence of the competitive layer.

The degree of alignment of the (002) orientation in the films was determined mainly by the deposition pressure. The narrowest rocking curve FWHMs were obtained for films grown with pressures below 1.33 Pa. However, the wide angle scans for these films show broadening and shifting of the (002) peak. The (002) peak for the 0.40 and 0.67 Pa films can be deconvoluted into two peaks, a higher intensity narrow peak shifted to 33.8° and a lower intensity broader peak at 34.3°, consistent with the observed bimodal distribution of (002) oriented grains shown in Fig. 8. The cross-sectional TEM in Fig. 7 shows that the bimodal distribution of grain sizes persists through the whole of the film to the substrate interface.

The differences observed in the film microstructure at different deposition pressures can be attributed to energy losses of the atomic species at the substrate due to collisions in the plasma sheath. The thickness of the plasma sheath at the substrate is estimated to be ~0.18 cm. This value is obtained assuming a plasma density at the sheath edge of $\sim 10^9$ cm^{-3} and a floating potential of ~30 V. This sheath thickness is the same order of magnitude as the estimated mean free path of the ionized flux of target material to the substrate. Increasing the pressure reduces the mean free path and increases the probability of collisions. Because Ar^+ has a larger momentum transfer cross-section than the oxygen ions, Ar^+ is expected to experience a greater number of energy reducing collisions. This is supported by the IEDs in Fig. 3, where the Ar^+ IED terminates at lower energies than the O^+, O_2^+, and O^{2+} IEDs. At pressures greater than 1.33 Pa, O^+ ions experience multiple collisions before reaching the substrate but still can arrive with enough energy to enhance the surface mobility but with minimal damage to the growing crystals. At this pressure, the ZnO films were dense with a smooth (002) textured surface and about 6 nm RMS roughness. By shortening the distance between the substrate and target, the plasma density is increased. This decreases the sheath width reducing the number of collisions resulting in higher energy of the ionized flux at the substrate and increasing the surface mobility of the adatoms on the substrate. These conditions promote favorable growth of the low energy (002) orientation, reducing the initial competitive layer of mixed (101) and (002) orientations. This is expected to be beneficial for reducing charge carrier scattering in the interfacial layer for ZnO TFT devices with back-gated architectures.

4. Conclusions

HiPIMS growth of ZnO films in an argon–oxygen environment resulted in films with predominantly (002) texture. Three microstructural phenomena were observed by changing the deposition parameters; an increase in the degree of (002) orientation, a bimodal size distribution of the (002) grains and a competitive (101)/(002) mixed texture layer at the substrate interface. Deposition pressure was found to have the strongest effect on the degree of (002) orientation. Lower pressures resulted in a higher degree of (002) orientation, however, at pressures below 0.93 Pa a bimodal distribution of grain sizes was observed, and optimum pressure of 1.33 Pa was found to provide dense and smooth films with (002) texture. The magnitude of the initial (101)/(002) competitive layer was independent of pressure, and is significantly diminished by reducing the substrate-to-target distance. These differences in microstructure can be attributed to the collisional energy exchanges of ion fluxes prior to arrival at the substrate, which attenuates the energy distributions of the ionized energetic species. This study helped demonstrate a low temperature growth of highly (002) textured, smooth, and dense ZnO films when using high energy ion fluxes from the HiPIMS process.

Acknowledgments

The authors would like to thank A.J. Safriet, N.R. Glavin, R.D. Smith, M.L. Jespersen, M. E. McConney, A.R. Waite, M.H. Check and K.D. Leedy for their support. Financial support from the Air Force Office of Scientific Research Aerospace Materials for Extreme Environments program (14RX13COR) is gratefully acknowledged.

References

[1] Divine Ngwashi Khan, Zinc Oxide Thin-Film Transistors: An Investigation of the Performance and Stability of Zinc Oxide Thin-Film Transistors and the Role of High-k Dielectrics, LAP Lambert Academic Publishing, 2011.
[2] U. Ozgur, D. Hofstetter, H. Morkoc, ZnO devices and applications: A review of current status and future prospects, Proc. IEEE (2010) 1255.
[3] U. Ozgur, Y. Alivov, C. Liu, A. Teke, M.A. Reshchikov, S. Dogan, V. Avrutin, S. Cho, H. Morkoc, A comprehensive review of ZnO materials and devices, J. Appl. Phys. 98 (2005) 41301.
[4] M. Shimizu, T. Shiosaki, A. Kawabata, Growth of c-axis oriented ZnO thin films with high deposition rate on silicon by CVD method, J. Cryst. Growth 57 (1982) 94.
[5] K. Haga, M. Kamidaira, Y. Kashiwaba, T. Sekiguchi, H. Watanabe, ZnO thin films prepared by remote plasma-enhanced CVD method, J. Cryst. Growth 214–215 (2000) 77.
[6] W.J. Maeng, S.J. Kim, J.S. Park, K.B. Chung, H. Kim, Low temperature atomic layer deposited Al-doped ZnO thin films and associated semiconducting properties, J. Vac. Sci. Technol. B 30 (2012).
[7] J.L. Wang, P.Y. Yang, T.Y. Hsieh, C.C. Hwang, D.C. Shye, I.C. Lee, The effects of oxygen annealing on the electrical characteristics of hydrothermally grown zinc oxide thin-film transistors, Solid State Electron. 77 (2012) 72.
[8] S. Elzwawi, D.H.S. Kim, R. Heinhold, M. Lynam, G. Turner, J.G. Partridge, D.G. McCulloch, Device quality ZnO grown using a filtered cathodic vacuum arc, Phys. B Condens. Matter 407 (2012) 2903.
[9] R.J. Mendelsberg, S.H.N. Lim, D.J. Milliron, A. Anders, High rate deposition of high quality ZnO:Al by filtered cathodic arc, Mater. Res. Soc. Symp. Proc. (2012) 45.
[10] X.L. Xu, S.P. Lau, B.K. Tay, Structural and optical properties of ZnO thin films produced by filtered cathodic vacuum arc, Thin Solid Films 398–399 (2001) 244.
[11] C.F. Yu, C.W. Sung, S.H. Chen, S.J. Sun, Relationship between the photoluminescence and conductivity of undoped ZnO thin films grown with various oxygen pressures, Appl. Surf. Sci. 256 (2009) 792.
[12] A.V. Singh, R.M. Mehra, N. Buthrath, A. Wakahara, A. Yoshida, Highly conductive and transparent aluminum-doped zinc oxide thin films prepared by pulsed laser deposition in oxygen ambient, J. Appl. Phys. 90 (2001) 5661.
[13] S. Amirhaghi, V. Craciun, D. Craciun, J. Elders, I.W. Boyd, Low temperature growth of highly transparent c-axis oriented ZnO thin films by pulsed laser deposition, Microelectron. Eng. 25 (1994) 321.
[14] V. Craciun, J. Elders, J.G.E. Gardeniers, I.W. Boyd, Characteristics of high quality ZnO thin films deposited by pulsed laser deposition, Appl. Phys. Lett. 65 (1994) 2963.
[15] V. Craciun, J. Elders, J.G.E. Gardeniers, J. Geretovsky, I.W. Boyd, Growth of ZnO thin films on GaAs by pulsed laser deposition, Thin Solid Films 259 (1995) 1 (259).
[16] L. Han, F. Mei, C. Liu, C. Pedro, E. Alves, Comparison of ZnO thin films grown by pulsed laser deposition on sapphire and Si substrates, Physica E Low Dimens. Syst. Nanostruct. 40 (2008) 699.
[17] S.L. King, J.G.E. Gardeniers, I.W. Boyd, Pulsed-laser deposited ZnO for device applications, Appl. Surf. Sci. 96–98 (1996) 811.
[18] F.R. Blom, F.C.M. Van de Pol, G. Bauhuis, T.J.A. Popma, RF planar magnetron sputtered ZnO films. II. Electrical properties, Thin Solid Films 204 (1991) 365.
[19] F.C.M. Van de Pol, F.R. Blom, T.J.A. Popma, RF planar magnetron sputtered ZnO films. I. Structural properties, Thin Solid Films 204 (1991) 349.
[20] R. Menon, K. Sreenivas, V. Gupta, Influence of stress on the structural and dielectric properties of RF magnetron sputtered zinc oxide thin film, J. Appl. Phys. 103 (2008) 094903-1-9.
[21] K.K. Kim, J.H. Song, H.J. Jung, W.K. Choi, S.J. Park, J.H. Song, J.Y. Lee, Photoluminescence and heteroepitaxy of ZnO on sapphire substrate (0001) grown by rf magnetron sputtering, J. Vac. Sci. Technol. A 18 (2000) 2864.

Distribution Statement A. Approved for public release; distribution unlimited.

[22] J. Sang-Hun, K. Bong-Soo, L. Byung-Teak, Photoluminescence dependence of ZnO films grown on Si(100) by radio-frequency magnetron sputtering on the growth ambient, Appl. Phys. Lett. 82 (2003) 2625.
[23] L. Sanghun, C. Dongkeun, K. Won-Jeong, H. Moon-Ho, L. Woong, Ga-doped ZnO films deposited with varying sputtering powers and substrate temperatures by pulsed DC magnetron sputtering and their property improvement potentials, Appl. Surf. Sci. 258 (2012) 6537.
[24] S. Lee, D. Cheon, W.J. Kim, K.J. Ahn, W. Lee, Combined effect of the target composition and deposition temperature on the properties of ZnO:Ga transparent conductive oxide films in pulsed dc magnetron sputtering, Semicond. Sci. Technol. 26 (2011) 115007.
[25] S. Konstantinidis, A. Hemberg, J.P. Dauchot, M. Hecq, Deposition of zinc oxide layers by high-power impulse magnetron sputtering, J. Vac. Sci. Technol. B 25 (2007) 19.
[26] J.G. Partridge, E.L.H. Mayes, N.L. McDougall, M.M.M. Bilek, D.G. McCulloch, Characterization and device applications of ZnO films deposited by high power impulse magnetron sputtering (HiPIMS), J. Phys. D 46 (2013) 165105.
[27] B. Bayraktaroglu, K. Leedy, R. Neidhard, Microwave ZnO thin-film transistors, IEEE Electron Device Lett. 29 (2008) 1024.
[28] B. Bayraktaroglu, K. Leedy, Pulsed laser deposited ZnO for thin film transistor applications, ECS Trans. (2008) 61.
[29] B. Bayraktaroglu, K. Leedy, Ordered nanocrystalline ZnO films for high speed and transparent thin film transistors, Proceedings of the IEEE Conference on Nanotechnology IEEE Computer Society, 2011, p. 1450.
[30] M. Yeon-Keon, M. Dae-Yong, L. Sang-Ho, J. Chang-Oh, P. Jong-Wan, High performance thin film transistor with ZnO channel layer deposited by DCmagnetronsputtering, J. Nanosci. Nanotechnol. 8 (2008) 4557.
[31] U. Helmersson, M. Lattemann, J. Alami, J. Bohlmark, A.P. Ehiasarian, J.T. Gudmundsson, High power impulse magnetron sputtering discharges and thin film growth: A brief review, Proceedings, Annual Technical Conference - Society of Vacuum Coaters, 2005, p. 458.
[32] K. Sarakinos, J. Alami, S. Konstantinidis, High power pulsed magnetron sputtering: A review on scientific and engineering state of the art, Surf. Coat. Technol. 204 (2010) 1661.
[33] D. Horwat, A. Anders, Compression and strong rarefaction in high power impulse magnetron sputtering discharges, J. Appl. Phys. 108 (2010) 123306.
[34] A. Anders, J. Capek, M. Hala, L. Martinu, The recycling trap: A generalized explanation of discharge runaway in high-power impulse magnetron sputtering, J. Phys. D 45 (2012) 012003.
[35] M. Aiempanakit, A. Aijaz, D. Lundin, U. Helmersson, T. Kubart, Understanding the discharge current behavior in reactive high power impulse magnetron sputtering of oxides, J. Appl. Phys. 113 (2013) 133302.
[36] M. Aiempanakit, U. Helmersson, A. Aijaz, P. Larsson, R. Magnusson, J. Jensen, T. Kubart, Effect of peak power in reactive high power impulse magnetron sputtering of titanium dioxide, Surf. Coat. Technol. 205 (2011) 4828.
[37] P.Y. Jouan, L. Le Brizoual, M. Ganciu, C. Cardinaud, S. Tricot, M.A. Djouadi, HiPIMS ion energy distribution measurements in reactive mode, IEEE Trans. Plasma Sci. (2010) 3089.
[38] A. Anders, J. Andersson, A. Ehiasarian, High power impulse magnetron sputtering: Current–voltage-time characteristics indicate the onset of sustained self-sputtering, J. Appl. Phys. 102 (2007) 113303.
[39] C. Nouvellon, M. Michiels, J.P. Dauchot, C. Archambeau, F. Laffineur, E. Silberberg, S. Delvaux, R. Cloots, S. Konstantinidis, R. Snyders, Deposition of titanium oxide films by reactive High Power Impulse Magnetron Sputtering (HiPIMS): Influence of the peak current value on the transition from metallic to poisoned regimes, Surf. Coat. Technol. 206 (2012) 3542.
[40] A. Hecimovic, K. Burcalova, A.P. Ehiasarian, Origins of ion energy distribution function (IEDF) in high power impulse magnetron sputtering (HIPIMS) plasma discharge, J. Phys. 41 (2008) 095203.
[41] S. Mraz, J.M. Schneider, Energy distribution of O- ions during reactive magnetron sputtering, Appl. Phys. Lett. 89 (2006) 51502.
[42] S. Mraz, J.M. Schneider, Influence of the negative oxygen ions on the structure evolution of transition metal oxide thin films, J. Appl. Phys. 100 (2006) 123303.
[43] P. Pokorny, M. Misina, J. Bulir, J. Lancok, P. Fitl, J. Musil, M. Novotny, Investigation of the Negative Ions in Ar/O2 Plasma of Magnetron Sputtering Discharge with Al:Zn Target by Ion Mass Spectrometry, Plasma Process. Polym. 8 (2011) 459.
[44] M. Bowes, P. Poolcharuansin, J.W. Bradley, Negative ion Energy Distributions in Reactive HiPIMS, J. Phys. D 46 (2013) 045204.
[45] J. Hupkes, J.I. Owen, S.E. Pust, E. Bunte, Chemical etching of zinc oxide for thin-film silicon solar cells, ChemPhysChem 13 (2012) 66.
[46] J.W. Shin, J.Y. Lee, T.W. Kim, Y.S. No, W.J. Cho, W.K. Choi, Growth mechanisms of thin-film columnar structures in zinc oxide on p-type silicon substrates, Appl. Phys. Lett. 88 (2006) 91911.

Distribution Statement A. Approved for public release; distribution unlimited.